journal of the mechanical behavior of biomedical materials 133 (2022) 105329

Contents lists available at ScienceDirect

Journal of the Mechanical Behavior of Biomedical Materials

journal homepage: www.elsevier.com/locate/jmbbm

Measuring the elastic modulus of soft biomaterials using nanoindentation

Dichu Xu [a,b,*], Terence Harvey [a], Eider Begiristain [c], Cristina Domínguez [c], Laura Sánchez-Abella [c], Martin Browne [b], Richard B. Cook [a]

[a] National Centre for Advanced Tribology at Southampton (nCATS), University of Southampton, Southampton, SO17 1BJ, UK
[b] Bioengineering Science Research Group, University of Southampton, Southampton, SO17 1BJ, UK
[c] CIDETEC, Basque Research and Technology Alliance (BRTA), Parque Científico y Tecnológico de Gipuzkoa, Miramón Pasealekua, 196, Donostia-San, Sebastián, 20014, Spain

ARTICLE INFO

Keywords:
Nanoindentation
Soft materials
Hydrogel
Elastic modulus
Stiffness

ABSTRACT

The measurement of the elastic modulus of soft biomaterials via nanoindentation relies on the accurate determination of the zero-point of the tip-sample interaction on which the depth of penetration into the sample is based. Non-cantilever based nanoindentation systems were originally designed for hard materials, and therefore monitoring the zero-point contact presents a significant challenge for the characterisation of very soft biomaterials. This study investigates the ability of non-cantilever based nanoindentation to differentiate between hydrogels with elastic moduli on the order of single kiloPascals (kPa) using a bespoke soft contact protocol and low flexural stiffness of instrument. Polyethylene glycol (PEG) hydrogels were fabricated as a model system with a range of elastic moduli by varying the polymer concentration and degree of crosslinking. Elastic modulus values were calculated using the Oliver-Pharr method, Hertzian contact model, as well as a viscoelastic model to account for the time-dependent behaviour of the gels. The stiffness measurements were validated by measuring cantilever beams with the equivalent flexural stiffness to that of the PEG hydrogels being tested. The results demonstrated a high repeatability of the measurements, enabling differentiation between hydrogels with elastic moduli in the single kPa to hundreds of kPa range.

1. Introduction

Hydrogels are often hydrophilic, biocompatible and biodegradable, which makes them promising soft biomaterials for biomedical applications such as regenerative medicine (Slaughter et al., 2009; Lin and Anseth, 2009), tissue engineering (Neumann et al., 2016), medical implants (Haque et al., 2012; Seliktar, 2012), targeted drug delivery system (Knop et al., 2010) and wound healing (Xue et al., 2019; Hou et al., 2020). In general, synthetic hydrogels can bear significant stresses under large strains by adjusting their crosslinked structure, for example compressive stress up to tens of megapascals (MPa) can be accommodated under strains of 90–95% (Gong, 2010). In addition, their physically/chemically crosslinked biphasic network can be tailored to provide an excellent environment for cell culture (Tibbitt and Anseth, 2009).

One of the major challenges in the field of the synthetic soft biomaterials is the ability to precisely control the mechanical properties of soft biomaterials to meet specific clinical needs, for example by varying permeability and/or swelling ratio (Huth et al., 2019). However, obtaining accurate mechanical property measurements is a challenging undertaking due to the lack of standards for the characterisation of very soft materials (Rubiano et al., 2019).

Currently, conventional techniques such as compression and tensile testing methods are used to characterise these materials (Burke et al., 2019; Cao et al., 2019; Zant et al., 2015; Cha et al., 2010; Huang et al., 2018; Khoushabi et al., 2018; Canillas et al., 2019; Fathi-Achachelouei et al., 2019; Wyss et al., 2020) usually performed at the macroscale, or atomic force microscopy (AFM) (Huth et al., 2019; Zhu et al., 2011; Suriano et al., 2016; Esteki et al., 2020) performed at the nano/-submicron scale. However, the modulus values of soft materials determined by different techniques can span three orders of magnitude at different length scales (Huth et al., 2019; Burke et al., 2019; Cao et al., 2019; Zant et al., 2015; Cha et al., 2010; Huang et al., 2018; Khoushabi et al., 2018; Canillas et al., 2019; Fathi-Achachelouei et al., 2019; Wyss et al., 2020; Zhu et al., 2011; Suriano et al., 2016; Esteki et al., 2020; Strange and Oyen, 2012; Kalcioglu et al., 2012).

* Corresponding author. National Centre for Advanced Tribology at Southampton (nCATS), University of Southampton, Southampton, SO17 1BJ, UK.
E-mail address: D.Xu@soton.ac.uk (D. Xu).

https://doi.org/10.1016/j.jmbbm.2022.105329
Received 5 October 2021; Received in revised form 14 June 2022; Accepted 18 June 2022
Available online 21 June 2022

Instrumented nanoindentation has been widely used to quantitatively analyse the mechanical properties of metals and thin films with elastic-plastic behaviour based on their force-displacement response (Fischer-Cripps, 2011). In contrast to macroscopic methods or AFM-based nanoindentation, the testing length scale can vary from the microns range down to the submicron/nanometre range, enabling assessment of both surface and bulk properties of materials, with a high-spatial resolution depending on the geometry of the indenter tip used (Tsui and Pharr, 1999). Recently, nanoindentation has been applied to soft materials with elastic moduli in the range below 10 kPa to hundreds of kPa (e.g. Optics11 indenter (Islam and Oyen, 2021), and others (Swain et al., 2017; Jiri et al., 2014; Carrillo et al., 2005; Ebenstein and Pruitt, 2004)), however, differentiating soft biomaterials with an elastic moduli of the order of single kilopascals using non-cantilever based nanoindentation systems remains challenging.

The accuracy of nanoindentation relies on the system's ability to correctly determine the area of contact between the tip and the material during the indentation cycle. This in turn relies on the determination of the zero-point, or the point at which the tip contacts the sample surface, so the depth of penetration can be accurately determined. In all commercially available non-cantilever based systems, movement of the tip requires some form of actuation, with the resistance to this movement coming from the deformation of the supporting springs between the frame and the tip holder. The flexural stiffness of the system derives from the stiffness of these springs, with the load vs. deformation of the springs normally determined through calibrations and removed from the indentation data during the analysis. For soft materials with modulus values in the kPa range, it can be difficult to determine the zero-point as the flexural stiffness of the measurement system (~100–167 N/m (Huan et al., 2010; Keysight Technologies, *n.d.*; Wang et al., 2015)) is much higher than the contact stiffness of tip-sample interaction (~1 N/m). Other techniques are in development such as microelectromechanical systems based scanning probe microscope (MEMS-SPM) which offer lower flexural stiffness values in the region of 13 N/m (Zhi Li et al., 2019).

The issue with high flexural stiffness when testing soft materials is that the system relies on being able to detect when additional resistance to the tip movement begins, over and above the resistance due to the spring deformation. When the flexural stiffness is high and the sample modulus is low, the initial contact and the change in resistance may not be discernible until the tip has penetrated many microns into the surface. This causes two issues; the first is the registration of the surface location during the pre-indentation setup and the second is the registration of the surface required for determination of the zero-point. The first can result in the additional penetration of the tip into the material surface which after sample positioning can result in the tip already being in contact with the surface when the indentation starts. The second can result in the false registration of the zero-point, with the tip having penetrated into the surface before the zero-point is assigned, resulting in a false area of contact and subsequent incorrect measures of the modulus and hardness values.

Apart from the zero-point determination, there are additional challenges in the nanoindentation testing of extremely soft biomaterials. The first is that there is no standard model for data processing of soft biomaterials; so far, the Oliver-Pharr method (Drira and Yadavalli, 2013) and Hertzian analysis (Swain et al., 2017) have been used in different studies, and these may produce inconsistent results. Furthermore, soft biomaterials show time-dependent mechanical behaviours (i.e. viscoelasticity and poroelasticity), which require dynamic mechanical analysis and more sophisticated data analysis techniques (Lai and Hu, 2018; Nagy et al., 2004; Feng and Ngan, 2002). The second is a lack of a standard soft material with known mechanical properties for calibration and verification. Standard reference materials such as fused silica have been commonly used for the calibration of hard materials. Although there are commercially available hydrogel samples for calibration (e.g. Petrisoft™ 35 mm Dish Easy Coat hydrogel), there is batch-to-batch variability in soft materials, which would affect the repeatability of the calibration process (Ebenstein and Pruitt, 2004). In addition, the determination of elastic modulus of Petrisoft™ gels was obtained using the Hertz model with an assumed Poisson's ratio value. The Hertz model suffers from the limitations, for example, the time-dependent behaviour of the hydrogel is not considered. The Poisson's ratio can vary with hydrogel composition, which results in variability in the stiffness calibration. Therefore, alternative calibration techniques are still required for the stiffness calibration in low stiffness range.

This study investigates the ability of a non-cantilever based nanoindentation system to determine the elastic moduli of hydrogels with elastic moduli in the single kPa range by utilising a 'soft contact protocol'. To verify these findings, a new calibration procedure is presented that uses cantilever beams of equivalent stiffness to the hydrogels under investigation. The nanoindentation results are examined using the Oliver-Pharr method, Hertzian model, as well as an elastic-viscoelastic model to account for the time-dependent behaviour of the hydrogels.

2. Materials

Pre-polymerised mixtures were produced using a combination of poly[(ethylene glycol) methacrylate] (PEG-MA, Mn = 360 Da, Sigma-Aldrich Co.) as a monomer, and poly(ethylene glycol) dimethacrylate (PEG-DMA, Mn = 550 Da, Sigma-Aldrich Co.) as a cross-linking agent. To determine the effect of cross-linking level on modulus value, PEG mixtures were prepared with 5, 10, 20 wt% of the cross-linking agent. PEG hydrogel samples were fabricated from 10, 20, 40 wt% PEG mixtures in phosphate buffered saline (PBS) in a climate chamber at 70 °C and 98% humidity for 2 h. The thermal free-radical polymerisation was initiated by ammonium persulfate (APS, Sigma-Aldrich Co.) with a molecular weight and purity of 228.20 g/mol and ≥99.99%, respectively. The code name of each specimen denotes the mass fraction of PEG mixture (wt%) in PBS, followed by the PEGMA:PEGDMA ratio. For example, "10.95.5" denotes the mass fraction of the PEG mixture in PBS is dissolved at 10 wt% where 95 wt% of PEGMA is mixed with 5 wt% of PEGDMA prior to polymerisation. The hydrated samples were around 7 mm in diameter and 2 mm thick. The formulations and mass swelling ratio of PEG-based hydrogel samples are listed in Table 1.

3. Methodology for nanoindentation testing

3.1. Nanoindentation test setup

The nanoindentation experiments were performed using a NanoTest Vantage system (MicroMaterials Ltd., Wrexham). A 500 μm radius spherical diamond tip was used as this allows for a large area of contact even at shallow indentation depths to overcome the discrepancies in measurements due to the surface roughness and heterogeneity in the hydrogel materials. A schematic of the indenter interacting with the hydrogel is shown in Fig. 1.

The test system is a pendulum based nanoindentation system and it provides a low flexural stiffness (~8 N/m). Prior to testing, a fully swollen PEG hydrogel specimen was adhered to the sample stub using a cyanoacrylate adhesive. A liquid cell set up allowed the hydrogels to be fully immersed in PBS solution, ensuring they were in a fully hydrated state before and during testing (MicroMaterials, *n.d.*). All tests were run in a temperature-controlled environment (20 ± 1 °C).

3.2. Soft contact protocol

Traditionally, non-cantilever nanoindentation systems identify the location of the sample's surface prior to testing by bringing the tip and the surface into contact, with the system determining the contact when a load of 10 μN is detected. Once detected, the system moves both the tip and the sample into a predefined measurement position which maximises the indentation depth measurable and places the tip 500 nm from

Table 1
PEG-based hydrogel material properties with varying concentration and crosslinking degree.

Code	10.95.5	10.90.10	10.80.20	20.95.5	20.90.10	20.80.20	40.95.5	40.90.10	40.80.20
PEG content (wt%)	10	10	10	20	20	20	40	40	40
PEGMA/PEGDMA Ratio	95:5	90:10	80:20	95:5	90:10	80:20	95:5	90:10	80:20
Mass swelling ratio (%)	97 ± 0.47	95 ± 0.06	94 ± 36	89 ± 0.02	88 ± 0.00	88 ± 0.14	78 ± 0.05	74 ± 0.00	75 ± 0.13

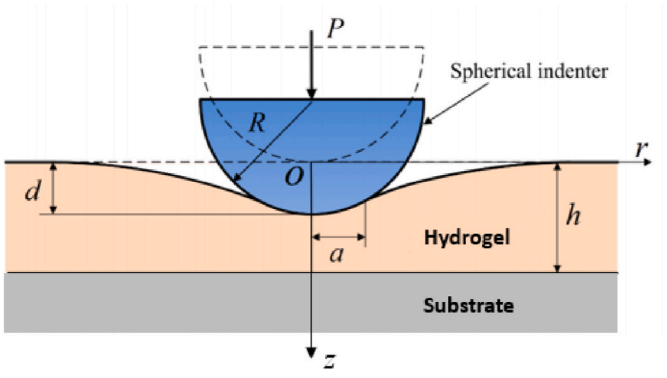

Fig. 1. A schematic representation of a spherical indenter contacting with hydrogel specimen, adapted from reference (Ding et al., 2018). The applied load is *P*, the radius of the spherical indenter is *R*, the radius of the circle of contact is *a*, the total penetration depth is *d*, and the thickness of hydrogel specimen *h*.

the detected 'surface position'. However, for materials with moduli in the kPa range, the tip may penetrate multiple microns into the surface prior to a 10 μN load being detected, resulting in the tip remaining in contact with the surface at the predefined measurement position.

The soft contact protocol attempted to address two issues: (i) finding the surface position during the pre-indentation setup and (ii) finding the zero-point to determine the accurate indentation depth.

This protocol allows the user to define a new measurement position, up to 50 μm from the detected 'surface position' (called initial tip-surface offset distance), ensuring the tip is clear of the sample surface prior to indentation. To enhance the accuracy of the zero-point determination, the protocol removes the 10 μN load based automatic zero-point determination and acquires load vs depth data collection from the onset of the indenter approach to the sample. This allows the user to determine the zero-point manually post-test. When the tip is travelling in the liquid before the tip-sample contact, the test force and the tip displacement are coupled by the supporting springs.

The flexural stiffness of the system derives from the stiffness of the supporting springs, with the load vs. deformation of the springs normally determined through calibrations post-indentation and removed from the raw indentation data during the analysis. The evolution of the contact stiffness *S* can be obtained from the test force vs. tip displacement post-indentation ($S = dF/dh$) when the flexural stiffness is removed from the raw load and displacement data (Fig. 2). The removal of the flexural stiffness flattens the contact stiffness curve before the initial tip-sample contact. The new zero-point is determined manually by detecting the start point of the continuous increase in the contact stiffness of the tip-sample interaction (Fig. 2).

3.3. Experimental setup

The nanoindentation tests were performed in load control to a maximum load (between 300 and 500 μN), with a 120 s hold at maximum load; loading and unloading rates were set at 1 μN/s and 5 μN/s respectively. This process of slow loading, more rapid unloading and long hold period was implemented to account for the viscoelastic and poroelastic behaviour of the hydrogels (Bush et al., 2015). The

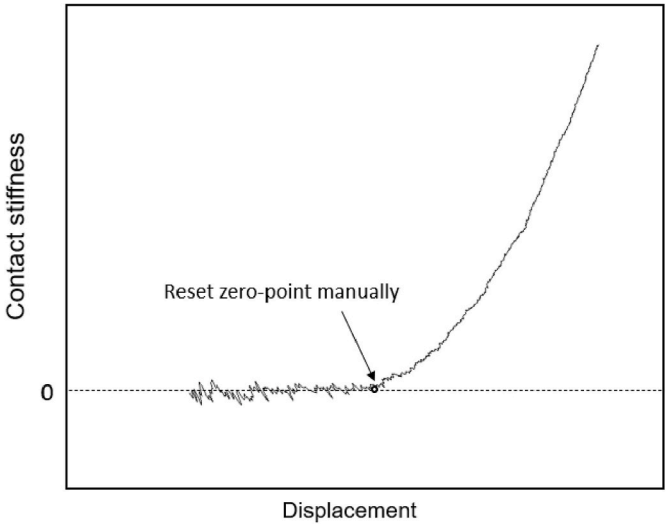

Fig. 2. Contact stiffness evolution during the tip movement.

indentation loading was set to terminate at either the maximum load or 28 μm indentation depth (which is slightly less than the full measurement range of 28.9 μm for the NanoTest Vantage system). Thirty indentations were performed on each of the hydrogel samples (3 samples for each PEG composition) with a minimum indent spacing of 300 μm, giving a total of 90 indents for each PEG composition.

3.4. Data analysis

3.4.1. Oliver-Pharr method

The system outputs a value known as the reduced modulus E_r, which takes into account the Young's modulus of the diamond indenter and the specimen, as expressed in equation (1)

$$\frac{1}{E_r} = \frac{1-\upsilon_i^2}{E_i} + \frac{1-\upsilon_s^2}{E_s} \tag{1}$$

where, E_r denotes the reduced modulus, E_i is the Young's modulus of the indenter (1141 GPa for diamond indenter), E_s is the Young's modulus of the specimen, υ_i is the Poisson's ratio of the indenter (0.07) and υ_s is the Poisson's ratio of the specimen. For soft materials, the indenter term in Equation (1) can be neglected as the compliance of the indenter is much less than the compliance of the soft materials, which leaves the reduced modulus (also called the effective modulus) $E_r = E_s/(1-\upsilon_s^2)$. Accurate values of the Poisson's ratio for these hydrogels were not known and would have varied with the composition as well as the level of crosslinking of the materials, thus, the reduced modulus values are reported in this study.

Based on the Oliver-Pharr method (Oliver and Pharr, 1992), for the spherical indenter, the reduced modulus can be calculated from the contact stiffness and the contact area at the penetration depth

$$E_r = \frac{\sqrt{\pi}}{2}\frac{S}{\sqrt{A}} \tag{2}$$

where *S* is the contact stiffness between the tip and the sample, which can be obtained by fitting the upper portion of the unloading curve with

a linear fit; A is the area of contact between the indenter and the sample.

3.4.2. Hertz model

Another widely used model for analysing the nanoindentation measurements of soft materials is the Hertz model. When using a spherical tip with a radius of R, the force-displacement data during the loading response are fitted to the Hertzian elastic loading response (Kontomaris and Malamou, 2020), as expressed in equation (3)

$$P = \frac{4}{3} E_r R^{1/2} d^{3/2} \tag{3}$$

where P is the applied load, d is the displacement.

The Hertz model or the Oliver-Pharr analysis is based on the same underlying contact mechanics theory and can be applied for soft biomaterials with the following assumptions (Kontomaris and Malamou, 2020), (Long et al., 2011). Firstly, the samples can be regarded as isotropic and homogeneous materials presenting a linear elastic response. Secondly, the sample can be considered as an infinite half space. This means the sample thickness is large in comparison to other length scales (e.g. the indenter radius or contact depth). Thirdly, it is assumed that there is no adhesion and friction between the contacting surfaces.

3.4.3. Elastic-viscoelastic model

To account for the time-dependent mechanical behaviour of the hydrogels, the creep-displacement-time data were analysed using the analytical solutions for the elastic-viscoelastic correspondence previously developed by Oyen (2005) and Mattice et al. (2006), to obtain equilibrium modulus values.

The hydrogel viscoelasticity in the time domain was expressed by using an empirical Prony series, for example the creep compliance of hydrogel materials in load-controlled creep can be expressed using equation (4)

$$J(t) = C_0 - \sum_{i=1}^{j} C_i \exp(-t/\tau_i) \tag{4}$$

where J is the creep compliance in shear ($J = 1/G$), C_0, C_i are constants and $C_0 = 2\ G_\infty$, τ_i denotes the viscoelastic relaxation time.

For spherical indentation creep following the ramp load, the displacement-time function during the hold period can be given by equation (5)

$$h^{3/2}(t) = \frac{3P_{\max}(1-\upsilon)}{4\sqrt{R}} \{C_0 - \sum_{i=1}^{j} C_i \exp(-t/\tau_i) \mathrm{RCF}_i\} \tag{5}$$

where $\mathrm{RCF_i}$ is the "ramp correction factor", and can be expressed by equation (6)

$$\mathrm{RCF}_i = \frac{\tau_i}{t_R} [\exp(t_R/\tau_i) - 1] \tag{6}$$

where t_R is the ramp loading time. The final displacement $h(\infty)$ can be estimated using the empirical creep displacement function $h(\infty) = a(1\text{-}e^{-bt})$ which can be interpreted from the Kelvin-Voigt viscoelastic model (a, b are fitted constants) (Hackney et al., 2012). Thus, the equilibrium shear modulus G_∞ and reduced modulus $E_{r,\infty} = 2\ G_\infty/(1\text{-}\nu)$ can be determined based on equation (5).

3.5. Statistical analysis

Statistical analysis was performed on each sample and each penetration depth to determine the mean and standard deviation values. To identify if there is a statistically significant difference in two group comparisons, one-way ANOVA with Tukey's HSD post hoc test was employed between the groups. Statistical significance was achieved when p-values were less than 0.05.

3.6. Calibration of a cantilever beam

The calibration procedure for the soft contact protocol of nanoindentation used a cantilever beam made of thin polypropylene plastic film with the film thickness of 0.45 mm (RS Components Ltd.). The cantilever beam has a rectangular cross-sectional area with the width (W) of 1 mm and the height (H) of 0.45 mm (Fig. 3). To be fixed at a sloped end sample stub, the cantilever beam was glued to a flat end surface with the width of ~1 mm. To generate cantilever beams with different flexural stiffness, the length (L) of cantilever beam was changed to 20 mm, 25 mm, 30 mm, 35 mm, and 40 mm, as measured from the fixed end to the loading point. The spherical indenter tip with a radius of 50 μm was brought into contact with the cantilever at the free end under load control using the soft contact protocol, with both loading and unloading rates set to 5 μN/s. The deflection of the cantilever beam δ under the load P is given by equation (7) (Holbery et al., 2000):

$$\delta = \frac{4PL^3}{EWH^3} \tag{7}$$

where E is the Young's modulus of the polypropylene plastic film, E = 1.67 GPa. Rearranging Equation (7), the flexural stiffness k (or the "spring constant") of the cantilever beam can be determined by equation (8)

$$k = \frac{EWH^3}{4L^3} \tag{8}$$

Three tests were carried out at each length of cantilever beam, and the flexural stiffness of the cantilever beams was obtained by a linear fitting to the load-displacement data.

4. Results

Typical force-displacement curves for one of the hydrogel samples (40.90.10) are shown in Fig. 4a. Repeatable indentation curves were obtained when the protocol was applied at different locations on specimen. Fig. 4b shows typical force-displacement curves for three of the PEG hydrogels, with the indenter tip travelling a distance of ≈11–12 μm before contact was detected. The average E_r values were determined to be 3.28 kPa, 12.28 kPa and 154.59 kPa using the Oliver-Pharr (O–P) method for 10.90.10, 20.90.10 and 40.90.10 respectively.

4.1. Effect of PEG hydrogel mixture concentration

The average E_r values obtained from the O–P method were plotted

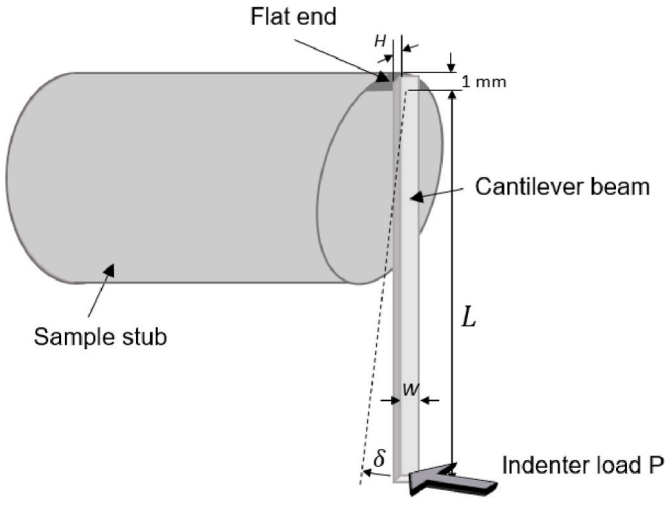

Fig. 3. A schematic of the cantilever beam with the length of L fixed at one end to a sample stub applied by the load P.

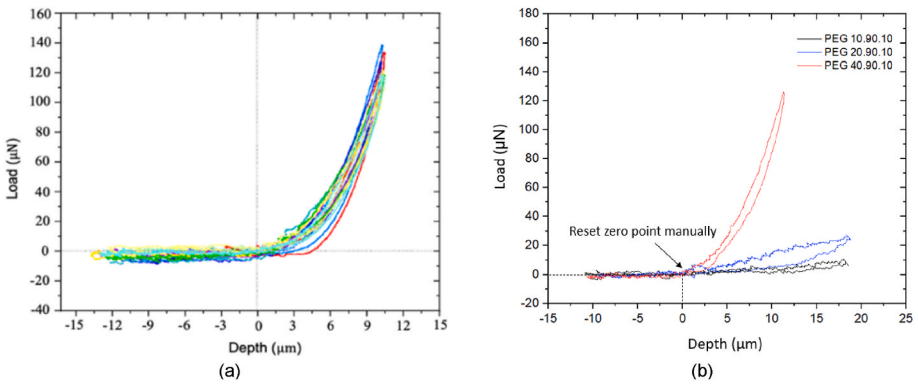

Fig. 4. Typical indent curves of PEG hydrogels (a) Ten indent curves obtained from different locations within one PEG hydrogel specimen of 40.90.10; (b) indentation curves from PEG specimen of 10.90.10, 20.90.10 and 40.90.10.

against the PEG concentrations (Fig. 5). The average E_r values for the 10 wt% PEG hydrogels were in the single kPa range (2.7–5.3 kPa), while significantly higher E_r values were found for the 40 wt% PEG hydrogels (28–205 kPa). For each PEGMA:PEGDMA ratio, the E_r values of the PEG hydrogels increased with increasing PEG concentration. The overall best fit for the E_r values with the PEG concentration without regard of various PEGMA:PEGDMA ratios had a corresponding power law of 2.2 (i.e. $E_r \propto c^b$, c denotes the total polymer concentration), with all differences being statistically significant between groups ($p < 0.001$). No statistically significant differences ($p > 0.05$) were found between samples of the same PEG composition indicating good repeatability in the measurement and protocol.

4.2. Effect of crosslinking

For all three models, the average E_r values increased with increasing concentrations of the cross-linker PEGDMA (5, 10, 20 wt%), with all differences between groups being statistically significant ($p < 0.001$) (Fig. 6). The trendlines of best fit for E_r with the crosslinker PEGDMA concentration were found to correspond to power laws for different PEG polymer concentrations, except for the 40.90.10 PEG samples deviating from the fit. The trend became steeper as the PEG polymer concentrations increased.

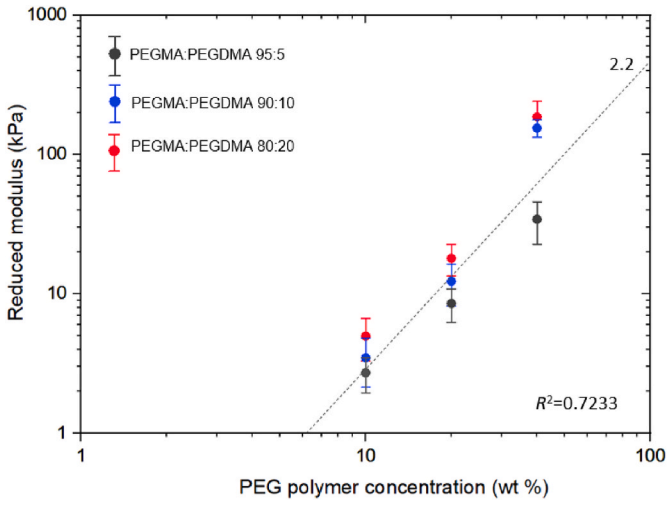

Fig. 5. Reduced moduli predicted by the O–P method as a function of PEG hydrogel concentrations (10, 20, 40 wt%). The black, blue and red circles denote the average E_r values of different crosslinker PEGDMA concentrations (5, 10, 20 wt %) in PEG polymer, and the error bars represent the standard deviation from 90 indentations for each PEG composition.

4.3. Effect of data analysis techniques

The O–P method predicted between 4% and 37% higher moduli values than the Hertz and viscoelastic models for all cases (Fig. 6). However, no statistically significant difference was found for the E_r values of the 10.95.5, 10.80.20, 20.80.20 PEG samples ($p > 0.05$) between the O–P method and the Hertz model. The equilibrium reduced modulus values ($E_{r,\infty}$) obtained from the viscoelastic model were consistently lower than the E_r values from the Hertzian model. Overall, the $E_{r,\infty}$ data showed higher standard deviations compared to those from the O–P method and Hertzian elastic analysis. However, the trendlines of best fit for E_r with the crosslinker PEGDMA concentration had similar power laws for all three models (Fig. 6).

4.4. Stiffness measurements of the cantilever beam

A range of stiffness values k (k = 0.59 N/m, 1.42 N/m, 2.45 N/m) were generated and compared with the nanoindentation results in Fig. 7a. Linear fitting of the load-displacement indentation curves gave flexural stiffnesses of $k_m = 0.56 \pm 0.03$ N/m, 1.42 ± 0.06 N/m, 2.37 ± 0.1 N/m, respectively. The stiffness was calculated and plotted as a function of the length of the cantilever beam and compared with the measured stiffness (Fig. 7b). The measured stiffness showed a good agreement with the calculated values as the errors were less than 10% in all tests, and the standard deviations of measurements were less than 5% of the average values.

The force-displacement curves for a cantilever with a nominal flexural stiffness of 0.59 N/m and a hydrogel (40.90.10) with a measured stiffness of 0.56 N/m (corresponding to a measured modulus of 3.28 kPa) were very similar (Fig. 8).

5. Discussion

This study has demonstrated the ability of nanoindentation to differentiate between hydrogels with elastic moduli on the order of single kPa and has verified this through measurements on cantilever beams of equivalent stiffness to the tested PEG hydrogels.

5.1. Calibration of the stiffness measurements

There is a lack of standard soft materials with known mechanical properties for calibrating indentation measurements on soft biomaterials. Firstly, although some commercial hydrogel materials with known stiffness are available (e.g. Petrisoft™ 35 mm Dish Easy Coat hydrogel), there is batch-to-batch variability which would affect the repeatability of the calibration process for super soft materials in the single kPa range. Secondly, the stiffness calibration of the commercial hydrogels was performed by applying Hertz's model with assumed

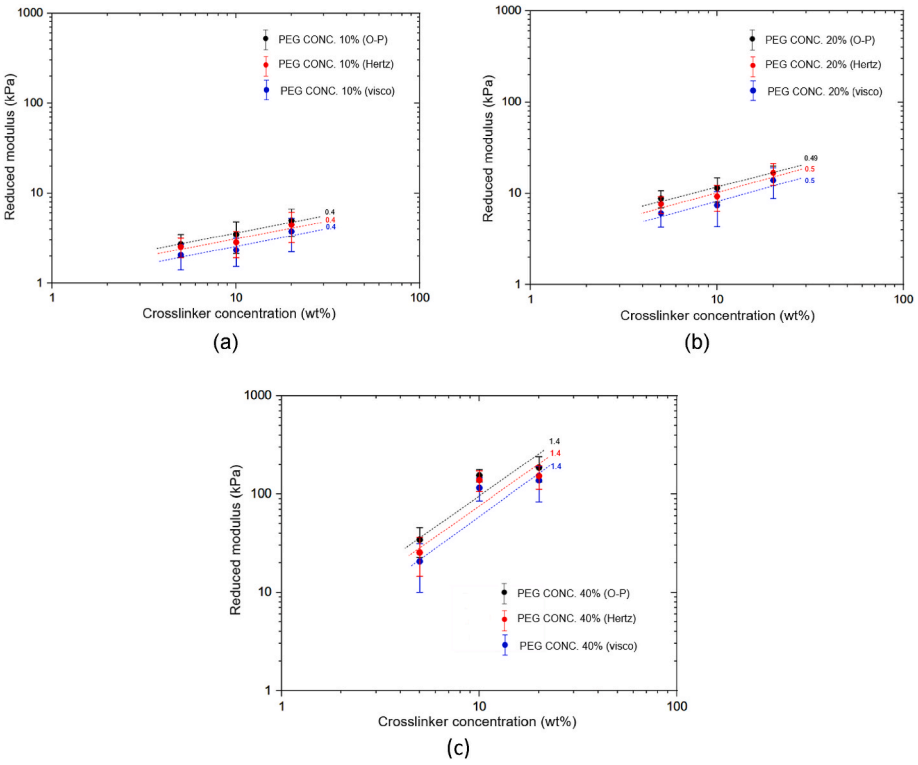

Fig. 6. Reduced moduli as a function of crosslinker PEGDMA concentrations in PEG polymer: (a) 5 wt %, (b)10 wt %, (c) 20 wt %. The circles denote the average E_r values and the error bars represent the standard deviations (90 indentations for each PEG composition).

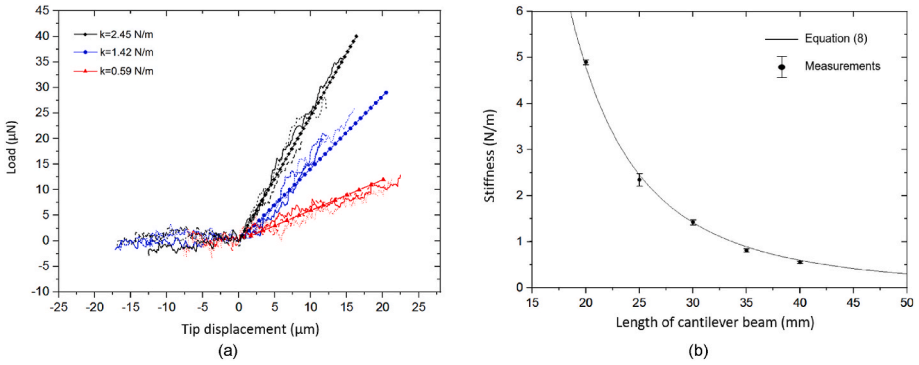

Fig. 7. The stiffness measurements of the cantilever beams using the soft contact protocol, compared to the stiffness values obtained using Equation (8). (a) Load versus tip displacement for variations in the cantilever length (red: 40 mm, blue: 30 mm, black: 25 mm); Solid, dot and dash lines were from three repeating tests and lines with circle markers were from calculations based on Equation (8); (b) Stiffness versus length of cantilever beams measured by nanoindentation in comparison with stiffness values obtained using Equation (8), the circle being the average values with error bars denoting standard deviations.

Poisson's ratio values. There are limitations of the Hertz's model on soft biomaterials which has been mentioned in Section 3.4.2. The Poisson's ratio can vary with the hydrogel compositions, which may cause the uncertainty in the stiffness calibration. In addition, the achieved stiffness calibration may not be reliable as the measured stiffness can be affected by the length scale of the measurements.

This study proposes a new calibration procedure that measured a range of flexural stiffnesses of cantilever beams, enabling the validation of nanoindentation measurements at low stiffness levels. This stiffness calibration method does not require the manufacture of hydrogels with a range of stiffness values. It can provide a range of stiffness levels by simply changing the length of cantilever beams. This method demonstrated high repeatability and results matched the analytically predicted stiffnesses well as both the errors and standard deviations were small (Fig. 7b). In addition, the calibration procedure also demonstrated the measured flexural stiffness of beams equivalent to the contact stiffness of the investigated hydrogels with elastic moduli at the single kPa level (Fig. 8). The hysteresis in the load-deflection curve is due to the small amount of creep when holding the load for 10 s after ramp loading.

5.2. Comparison with other testing methods

The elastic moduli of PEG-based hydrogels have been widely investigated using conventional macroscopic testing methods complied to compression and tension, microindentation and AFM, with the reported values of elasticity of PEG-based hydrogels in a broad range varying from 4 kPa to 1 MPa (Burke et al., 2019), (Khoushabi et al., 2018; Canillas et al., 2019), (Mignon et al., 2019; Rice and Anseth, 2004; Kolewe et al., 2018; Shapiro and Oyen, 2014; Gäbler et al., 2009; Lau et al., 2020). The E_r values presented in this study are of the same order of magnitude as the elastic moduli measured by compression/tensile tests reported in the literature for similar PEG hydrogel systems (Zant et al., 2015; Rice and Anseth, 2004; Mignon et al., 2019) (Fig. 9). As an example, at 10 wt% PEG concentration, the new protocol recorded E_r values of this study were between 2 and 7 kPa, compared to compressive modulus values of 4–12 kPa observed for compression tests on PEGDMA hydrogels (Rice and Anseth, 2004). As the compliance of the indenter is much less than the compliance of the soft materials, the indenter term contributing to the reduced modulus can be neglected. The reduced

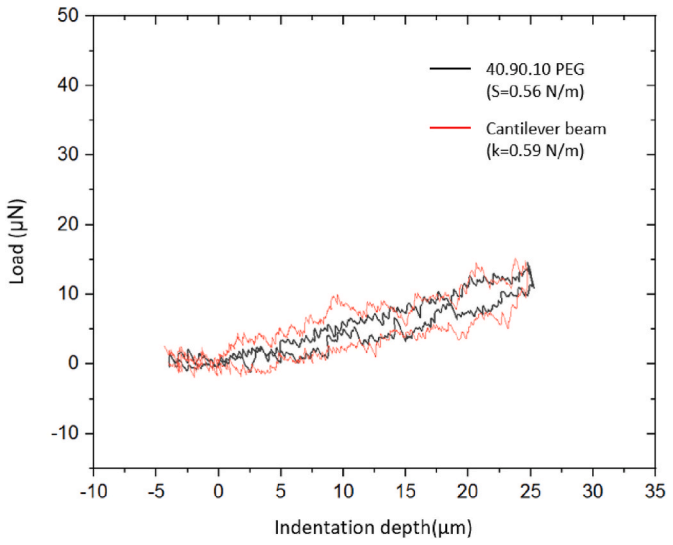

Fig. 8. Comparison of the nanoindentation curves from the cantilever beam with the flexural stiffness of 0.59 N/m and the 40.90.10 hydrogel with the contact stiffness of 0.56 N/m.

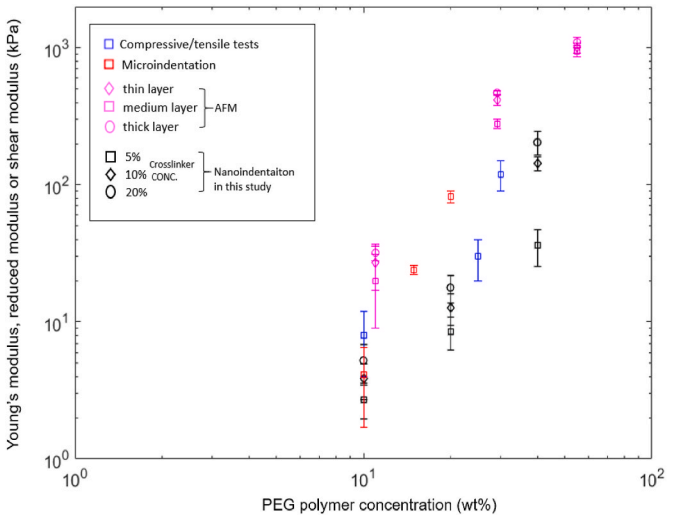

Fig. 9. The reported reduced moduli or Young's moduli of PEG-based hydrogel measured with different experimental techniques, compared with the values reported in this study. Data compiled from: Macroscopic testing method (Zant et al., 2015; Rice and Anseth, 2004; Mignon et al., 2019); AFM-based nanoindentation (Kolewe et al., 2018); Microindentation testing method (Shapiro and Oyen, 2014).

modulus will be very close to the elastic modulus of the soft materials. While the E_r values were reported instead of Young's modulus values as the Poisson's ratio for these hydrogels were not known, the E_r value can still be used for comparing the relative stiffnesses of different hydrogel materials.

While macroscopic compressive and tensile mechanical tests can measure moduli down to the single kPa scale, they are subject to a number of limitations. As the load and displacement resolution is relatively low, a large volume of material is often required at length scales of the order of millimetres. In addition, the specimen would be unusable after a single test. Secondly, specific size and the shape requirements present challenges in manufacturing accurately sized samples free from damage. Perhaps of most relevance to the current study, tensile tests present difficulties with 'gripping' soft specimens (Oyen, 2014).

Shapiro and Owen used microindentation to obtain shear modulus values for PEGDMA hydrogels (Shapiro and Oyen, 2014). They found elastic moduli comparable to this and other studies (Fig. 9), however, the standard deviations observed (~60%) were much higher than those values in this study (~25%, 40%, 32% for the three different crosslinking levels, respectively). Nanoindentation was also performed on the same 10 wt% PEGDMA gels by Shapiro and Oyen (2014), where they found much higher shear modulus values and standard deviations (14.6 ± 9.2 kPa) than those presented here.

The indenter tip used in microindentation is often of the order of several millimetres, which results in a contact area much larger than the length scale of the underlying hydrogel microstructure; thus, microindentation is not suitable for characterising heterogeneity within the materials. In addition, the size of the indenter tip used, restricts microindentation to a shallow depths of penetration and small strains (Rubiano et al., 2019).

In contrast to the macro and microscopic techniques mentioned above, nanoindentation techniques enable characterisation of soft biomaterials down nano-/micro-newton force and nanometre depth scale. In addition, there is no need for special preparation before testing and the sample volumes for testing are minimal.

AFM-based nanoindentation has the finest spatial resolution as it uses small probe sizes with radii ranging from tens of nm to several μm. However, the results can vary widely due to the surface characteristics (e.g. surface topography and roughness) (Huth et al., 2019). Young's modulus values from AFM-based nanoindentation tended to be higher than those measured by other techniques, especially for low modulus PEG hydrogels (Fig. 9). Similarly, soft PDMS samples can present Young's moduli up to two orders of magnitudes higher than those from microindentation and tensile tests (Megone et al., 2018). One of the origins for the discrepancy between local (nanoscale) and bulk properties has been attributed to the surface adhesion between the AFM tip and the samples surfaces (Megone et al., 2018). In addition, the penetration depth of the AFM probe into soft materials is very limited by the deflection of the cantilever (up to 10 μm (Markert et al., 2013)), and the inclination angle of the cantilever can cause an additional shearing force between the tip and the samples at deeper indentation depths (Huth et al., 2019). These factors limit AFM-based nanoindentation to characterisation of the surface and not bulk properties of samples. AFM-based nanoindentation is further complicated by the so-called "jump-in" effect. As the AFM probe approaches the sample, if the stiffness of the cantilever is much lower than the stiffness of the tip-sample interaction, the cantilever spontaneously jumps into contact with the sample. This results in a false detection of the initial contact point and consequent inaccuracy in the determination of the contact area (Sheiko and Magonov, 2012). This is a particular issue when assessing low modulus gels as low stiffness cantilevers must be used if they are to flex in contact.

In this study, the full measurement range of the indentation depth can be up to 28.9 μm, allowing the effects of surface properties to be obviated and enabling the assessment of the bulk properties of thick hydrogels. Note that no "jump into contact" phenomenon or adhesion effects were observed in the nanoindentation curves (Fig. 4).

5.3. *Effect of crosslinking and polymer concentration on the elastic moduli*

Selby et al. (2014) found a simple linear relationship between the elastic modulus and the concentration of crosslinker for poly(hydroxyethyl methacrylate) (pHEMA) specimens as the crosslinker concentration increased from 0.2 to 5%. This study found the relationship was more complex and dependent on both the crosslinker and total polymer concentration. The crosslinker concentration was observed to have a smaller effect on E_r than the PEG polymer concentration (Figs. 5 and 6), in agreement with a previous study (Oyen, 2014). Oyen (2014) used data from multiple studies on swollen gels to determine a power law relationship ($E_r \propto c^{2.25}$) between the elastic moduli and the total polymer

concentration similar to that observed in this study ($E_r \propto c^{2.2}$). Although there is a difference in the E_r values obtained from different data analysis techniques, the relationship between the elastic moduli and the crosslinker concentration was not affected according to the models, as evidenced by the parallel trendlines (Fig. 6).

5.4. Elastic and elastic-viscoelastic analyses

The Oliver-Pharr and Hertz models have been commonly used in the analyses of biological samples. For both models, the samples are approximately considered as homogeneous and isotropic materials and assumed as an infinite elastic half space. As such, the sample should be thick (i.e. $h \gg \sqrt{Rd}$), and the indentation depth should be small (i.e. the maximum indentation depth should not exceed 10% of the sample thickness according to Bückle's rule (Clifford and Seah, 2006)).

The Hertz model analyses the loading curve, while the Oliver-Pharr method uses the initial portion of the unloading curve and assumes only elastic recovery occurs during this phase. If the biological samples are isotropic, homogeneous, and purely elastic material, the loading and unloading curve will be identical and both models will yield the same results (Kontomaris and Malamou, 2020). However, the comparison between the E_r datasets derived from both models showed that the O–P model produces higher moduli values in all cases (Fig. 6). This discrepancy is comparable to that reported in literature (Kontomaris and Malamou, 2020).

It should be noted that there are limitations of Oliver-Pharr method for the soft biomaterials. Firstly, the unloading curve can be affected by the adhesion between the tip and the sample, which can influence the results. For this, the models such as Johnson-Kendall-Roberts (JKR) (Johnson et al., 1971) and Derjaguin-Muller-Toporov (DMT) (Derjaguin et al., 1975) should be considered. Secondly, the soft biomaterials show time-dependent behaviour (i.e. the creep behaviour), which results in a vertical or negative slope in the initial portion of unloading. Thus, high unloading rates and long hold periods are required to overcome this issue. In addition, some corrections on the unloading data have been applied for the Oliver-Pharr method to include the creep effect. Feng and Ngan (2002) presented a method by which the measured elastic modulus can be corrected for the effects of creep and thermal drift. Lower elastic modulus values were also obtained after the creep corrections. In this study, the displacement rate to the unloading rate ratio at the end of 120s holding time was very small (<2.15E-4 μm/μN) compared to the apparent contact compliance (~0.1 μm/μN for the stiffest gel investigated), which means the effects of creep and thermal drift on the apparent contact stiffness can be neglected.

The E_r values using the Hertzian model were closer to the equilibrium elastic moduli ($E_{r,\infty}$) obtained by the viscoelastic model (Fig. 6), while the E_r values produced by Hertz model were consistently higher than the $E_{r,\infty}$ values by taking into account the creep behaviour of the hydrogels.

The poroelastic behaviour of the hydrogels was not considered here, but this will not affect the output of the equilibrium elastic moduli using Equation (5), as the poroelastic effect on the contact stiffness would be zero at final creep displacement. However, for indentation on thin hydrogel layers, the substrate effect will significant increase the measured reduced modulus values. When large strains are performed, the linear elastic models cannot be used. Furthermore, the influence of the poroelasticity on the contact stiffness will increase with the strains (Degen et al., 2020), and thus, the poroelastic mechanical properties (i.e. diffusivity and permeability) should also be considered, especially for large strains on thin hydrogel layers. Future studies could look at those phenomena.

6. Conclusion

This study has demonstrated the ability of a non-cantilever based nanoindentation system to determine the elastic moduli of materials which are in the order of single kPa, providing a repeatability that enables differentiation between materials with stiffnesses of this magnitude. The Oliver-Pharr method produced statistically higher moduli values compared to the Hertz and viscoelastic models, while the relationship between the elastic moduli and the crosslinker concentration was not influenced by the analysis methods. In addition, the study has demonstrated a cantilever calibration method, to enable the validation of measurements at these low stiffness levels.

Funding information

This work was supported by funding from the European Union (EU) within its Horizon 2020 programme, project MDOT (Grant Agreement 814654).

CRediT authorship contribution statement

Dichu Xu: Writing – original draft, Validation, Methodology, Investigation, Formal analysis, Conceptualization. **Terence Harvey:** Writing – review & editing. **Eider Begiristain:** Resources. **Cristina Domínguez:** Resources. **Laura Sánchez-Abella:** Resources, Project administration. **Martin Browne:** Writing – review & editing, Supervision, Project administration, Funding acquisition, Conceptualization. **Richard B. Cook:** Writing – review & editing, Supervision, Project administration, Methodology, Funding acquisition, Conceptualization.

Declaration of competing interest

The authors declare that they have no known competing financial interests or personal relationships that could have appeared to influence the work reported in this paper.

Data availability

Data will be made available on request.

Acknowledgements

The authors would like to thank Adrian Harris (Micro Materials Ltd.) for the help with the nanoindentation testing. The authors are grateful to Dr Damien Dupin (CIDETEC) for proofreading the article. This work was supported by funding from the European Union (EU) within its Horizon 2020 programme, project MDOT (Grant Agreement 814654).

References

Burke, G., Cao, Z., Devine, D.M., Major, I., 2019. Preparation of biodegradable polyethylene glycol dimethacrylate hydrogels via thiol-ene chemistry. Polymers 11 (8). https://doi.org/10.3390/polym11081339.

Bush, B.G., Shapiro, J.M., DelRio, F.W., Cook, R.F., Oyen, M.L., 2015. Mechanical measurements of heterogeneity and length scale effects in PEG-based hydrogels. Soft Matter 11 (36), 7191–7200. https://doi.org/10.1039/c5sm01210d.

Canillas, M., et al., 2019. Photopolymerization for filling porous ceramic matrix: improvement of mechanical properties and drug delivering behavior. Polym. Compos. 40 (4), 1654–1662. https://doi.org/10.1002/pc.24914.

Cao, K., Flegg, D.S., Lin, S., Lagugné-Labarthet, F., Mequanint, K., Gillies, E.R., 2019. Fabrication and in situ cross-linking of carboxylic-acid-functionalized poly(ester amide) Scaffolds for tissue engineering. ACS Appl. Polym. Mater. 1 (9), 2360–2369. https://doi.org/10.1021/acsapm.9b00475.

Carrillo, F., et al., 2005. Nanoindentation of polydimethylsiloxane elastomers: effect of crosslinking, work of adhesion, and fluid environment on elastic modulus. J. Mater. Res. 20 (10), 2820–2830. https://doi.org/10.1557/JMR.2005.0354.

Cha, C., Kim, S.Y., Cao, L., Kong, H., 2010. Decoupled control of stiffness and permeability with a cell-encapsulating poly(ethylene glycol) dimethacrylate hydrogel. Biomaterials 31 (18), 4864–4871. https://doi.org/10.1016/j.biomaterials.2010.02.059.

Clifford, C.A., Seah, M.P., 2006. Modelling of nanomechanical nanoindentation measurements using an AFM or nanoindenter for compliant layers on stiffer substrates. Nanotechnology 17 (21), 5283–5292. https://doi.org/10.1088/0957-4484/17/21/001.

Degen, G.D., Chen, Y.T., Chau, A.L., Månsson, L.K., Pitenis, A.A., 2020. Poroelasticity of highly confined hydrogel films measured with a surface forces apparatus. Soft Matter 16 (35), 8096–8100. https://doi.org/10.1039/d0sm01312a.

Ding, Y., Yuan, W.K., Wang, G.F., 2018. Spherical indentation on biological films with surface energy. J. Phys. D Appl. Phys. 51 (29) https://doi.org/10.1088/1361-6463/aacaec, 0–6.

Drira, Z., Yadavalli, V.K., 2013. Nanomechanical measurements of polyethylene glycol hydrogels using atomic force microscopy. J. Mech. Behav. Biomed. Mater. 18, 20–28. https://doi.org/10.1016/j.jmbbm.2012.09.015.

Ebenstein, D.M., Pruitt, L.A., 2004. Nanoindentation of soft hydrated materials for application to vascular tissues. J. Biomed. Mater. Res., Part A 69 (2), 222–232. https://doi.org/10.1002/jbm.a.20096.

Esteki, M.H., Alemrajabi, A.A., Hall, C.M., Sheridan, G.K., Azadi, M., Moeendarbary, E., 2020. A new framework for characterization of poroelastic materials using indentation. Acta Biomater. 102, 138–148. https://doi.org/10.1016/j.actbio.2019.11.010.

Fathi-Achachelouei, M., Keskin, D., Bat, E., Vrana, N.E., Tezcaner, A., 2019. Dual growth factor delivery using PLGA nanoparticles in silk fibroin/PEGDMA hydrogels for articular cartilage tissue engineering. no. December 2019 J. Biomed. Mater. Res. Part B Appl. Biomater. 2041–2062. https://doi.org/10.1002/jbm.b.34544.

Feng, G., Ngan, A.H.W., 2002. Effects of creep and thermal drift on modulus measurement using depth-sensing indentation. J. Mater. Res. 17 (3), 660–668. https://doi.org/10.1557/JMR.2002.0094.

Fischer-Cripps, A.C., 2011. Nanoindentation. Springer, New York.

Gäbler, S., et al., 2009. Determination of the viscoelastic properties of hydrogels based on polyethylene glycol diacrylate (PEG-DA) and human articular cartilage. Int. J. Mater. Eng. Innovat. 1 (1), 3–20. https://doi.org/10.1504/IJMATEI.2009.024024.

Gong, J.P., 2010. Why are double network hydrogels so tough? Soft Matter 6 (12), 2583–2590. https://doi.org/10.1039/b924290b.

Hackney, S.A., Aifantis, K.E., Tangtrakarn, A., Shrivastava, S., 2012. Using the Kelvin-Voigt model for nanoindentation creep in Sn-C/PVDF nanocomposites. Mater. Sci. Technol. 28 (9–10), 1161–1166. https://doi.org/10.1179/1743284712Y.0000000063.

Haque, M.A., Kurokawa, T., Gong, J.P., 2012. Super tough double network hydrogels and their application as biomaterials. Polymer 53 (9), 1805–1822. https://doi.org/10.1016/j.polymer.2012.03.013.

Holbery, J.D., Eden, V.L., Sarikaya, M., Fisher, R.M., 2000. Experimental determination of scanning probe microscope cantilever spring constants utilizing a nanoindentation apparatus. Rev. Sci. Instrum. 71 (10), 3769–3776.

Hou, Y., et al., 2020. A fast UV-curable PU-PAAm hydrogel with mechanical flexibility and self-adhesion for wound healing. RSC Adv. 10 (9), 4907–4915. https://doi.org/10.1039/c9ra10666a.

Huan, Y., Liu, D., Yang, R., Zhang, T., 2010. Analysis of the Practical Force Accuracy of Electromagnet-Based Nanoindenters," *Measurement*. Journal of the International Measurement Confederation. https://doi.org/10.1016/j.measurement.2010.04.005 [Online]. Available.

Huang, H., Tan, Y., Ayers, D.C., Song, J., 2018. Anionic and zwitterionic residues modulate stiffness of photo-cross-linked hydrogels and cellular behavior of encapsulated chondrocytes. ACS Biomater. Sci. Eng. 4 (5), 1843–1851. https://doi.org/10.1021/acsbiomaterials.8b00124.

Huth, S., Sindt, S., Selhuber-Unkel, C., 2019. Automated analysis of soft hydrogel microindentation: impact of various indentation parameters on the measurement of Young's modulus. PLoS One 14 (8), 1–17. https://doi.org/10.1371/journal.pone.0220281.

Islam, M.R., Oyen, M.L., 2021. A poroelastic master curve for time-dependent and multiscale mechanics of hydrogels. J. Mater. Res. https://doi.org/10.1557/s43578-020-00090-5.

Jiri, N., Michael, S., Philipp, E., 2014. Micromechanical properties of polyacrylamide hydrogels measured by spherical nanoindentation. Key Eng. Mater. 606, 121–124. https://doi.org/10.4028/www.scientific.net/KEM.606.121.

K, K., Kenneth Langstreth Johnson, A.D.R., 1971. Surface energy and the contact of elastic solids. Proc. R. Soc. London. A. Math. Phys. Sci. 324 (1558), 301–313. https://doi.org/10.1088/0022-3727/6/9/304.

Kalcioglu, Z.I., Mahmoodian, R., Hu, Y., Suo, Z., Van Vliet, K.J., 2012. From macro- to microscale poroelastic characterization of polymeric hydrogels via indentation. Soft Matter 8 (12), 3393–3398. https://doi.org/10.1039/c2sm06825g.

Keysight Technologies. Keysight Technologies Nano Indenter G200 Precise Mechanical Testing for Micro-to-nano Range of Loads and Displacements. Data Sheet. Assessed: June 2021 [Online]. Available: https://www.keysight.com/us/en/assets/7018-02195/data-sheets-archived/5990-4172.pdf.

Khoushabi, A., Wyss, C.S., Caglar, B., Pioletti, D., Bourban, P.E., 2018. Tailoring swelling to control softening mechanisms during cyclic loading of PEG/cellulose hydrogel composites. Compos. Sci. Technol. 168, 88–95. https://doi.org/10.1016/j.compscitech.2018.08.043. February.

Knop, K., Hoogenboom, R., Fischer, D., Schubert, U.S., 2010. Poly(ethylene glycol) in drug delivery: pros and cons as well as potential alternatives. Angew. Chem. Int. Ed. 49 (36), 6288–6308. https://doi.org/10.1002/anie.200902672.

Kolewe, K.W., Zhu, J., Mako, N.R., Nonnenmann, S.S., Schiffman, J.D., 2018. Bacterial adhesion is affected by the thickness and stiffness of poly(ethylene glycol) hydrogels. ACS Appl. Mater. Interfaces 10 (3), 2275–2281. https://doi.org/10.1021/acsami.7b12145.

Kontomaris, S.V., Malamou, A., 2020. Hertz model or Oliver & Pharr analysis? Tutorial regarding AFM nanoindentation experiments on biological samples. Mater. Res. Express 7 (3). https://doi.org/10.1088/2053-1591/ab79ce.

Lai, Y., Hu, Y., 2018. Probing the swelling-dependent mechanical and transport properties of polyacrylamide hydrogels through AFM-based dynamic nanoindentation. Soft Matter 14 (14), 2619–2627. https://doi.org/10.1039/c7sm02351k.

Lau, H.K., et al., 2020. Micromechanical properties of microstructured elastomeric hydrogels. Macromol. Biosci. 1900360, 1–12. https://doi.org/10.1002/mabi.201900360.

Lin, C.C., Anseth, K.S., 2009. PEG hydrogels for the controlled release of biomolecules in regenerative medicine. Pharm. Res. (N. Y.) 26 (3), 631–643. https://doi.org/10.1007/s11095-008-9801-2.

Long, R., Hall, M.S., Wu, M., Hui, C.Y., 2011. Effects of gel thickness on microscopic indentation measurements of gel modulus. Biophys. J. 101 (3), 643–650. https://doi.org/10.1016/j.bpj.2011.06.049.

Markert, C.D., et al., 2013. Characterizing the micro-scale elastic modulus of hydrogels for use in regenerative medicine. J. Mech. Behav. Biomed. Mater. 27, 115–127. https://doi.org/10.1016/j.jmbbm.2013.07.008.

Materials, Micro. How it works Liquid cell applications and investigating of soft materials immersed in liquids includes : investigate a wide range of stiffness values. Accessed: June 2022 [Online]. Available: https://www.micromaterials.co.uk/environment/liquid-cell/.

Mattice, J.M., Lau, A.G., Oyen, M.L., Kent, R.W., 2006. Spherical indentation load-relaxation of soft biological tissues. J. Mater. Res. 21 (8), 2003–2010. https://doi.org/10.1557/jmr.2006.0243.

Megone, W., Roohpour, N., Gautrot, J.E., 2018. Impact of surface adhesion and sample heterogeneity on the multiscale mechanical characterisation of soft biomaterials. Sci. Rep. 8 (1), 1–10. https://doi.org/10.1038/s41598-018-24671-x.

Mignon, A., et al., 2019. Combined effect of Laponite and polymer molecular weight on the cell-interactive properties of synthetic PEO-based hydrogels. January React. Funct. Polym. 136, 95–106. https://doi.org/10.1016/j.reactfunctpolym.2018.12.017.

Nagy, A., et al., 2004. Mechanical spectroscopy of thin layers of PPV polymer on Si substrates. Mater. Sci. Eng., A 370 (1–2), 311–315. https://doi.org/10.1016/j.msea.2003.08.082.

Neumann, A.J., Quinn, T., Bryant, S.J., 2016. Nondestructive evaluation of a new hydrolytically degradable and photo-clickable PEG hydrogel for cartilage tissue engineering. Acta Biomater. 39, 1–11. https://doi.org/10.1016/j.actbio.2016.05.015.

Oliver, W.C., Pharr, G.M., 1992. An improved technique for determining hardness and elastic modulus using load and displacement sensing indentation experiments. J. Mater. Res. 7 (6), 1564–1583.

Oyen, M.L., 2005. Spherical indentation creep following ramp loading. J. Mater. Res. 20 (8), 2094–2100. https://doi.org/10.1557/JMR.2005.0259.

Oyen, M.L., 2014. Mechanical characterisation of hydrogel materials. Int. Mater. Rev. 59 (1), 44–59. https://doi.org/10.1179/1743280413Y.0000000022.

Rice, M.A., Anseth, K.S., 2004. Encapsulating chondrocytes in copolymer gels: bimodal degradation kinetics influence cell phenotype and extracellular matrix development. J. Biomed. Mater. Res., Part A 70 (4), 560–568. https://doi.org/10.1002/jbm.a.30106.

Rubiano, A., Galitz, C., Simmons, C.S., 2019. Mechanical characterization by mesoscale indentation: advantages and pitfalls for tissue and scaffolds. Tissue Eng. C Methods 25 (10), 619–629. https://doi.org/10.1089/ten.tec.2018.0372.

Selby, A., Maldonado-Codina, C., Derby, B., 2014. Influence of specimen thickness on the nanoindentation of hydrogels: measuring the mechanical properties of soft contact lenses. J. Mech. Behav. Biomed. Mater. 35, 144–156. https://doi.org/10.1016/j.jmbbm.2013.11.023.

Seliktar, D., 2012. Designing cell-compatible hydrogels for biomedical applications (80-.). Science 336 (6085), 1124–1128.

Shapiro, J.M., Oyen, M.L., 2014. Viscoelastic analysis of single-component and composite PEG and alginate hydrogels. Acta Mech. Sin. 30 (1), 7–14. https://doi.org/10.1007/s10409-014-0025-x.

Sheiko, S.S., Magonov, S.N., 2012. Scanning Probe Microscopy of Polymers, vol. 2. Elsevier B.V.

Slaughter, B.V., Khurshid, S.S., Fisher, O.Z., Khademhosseini, A., Peppas, N.A., 2009. Hydrogels in regenerative medicine. Adv. Mater. 21 (32–33), 3307–3329. https://doi.org/10.1002/adma.200802106.

Strange, D.G.T., Oyen, M.L., 2012. Composite hydrogels for nucleus pulposus tissue engineering. J. Mech. Behav. Biomed. Mater. 11, 16–26. https://doi.org/10.1016/j.jmbbm.2011.10.003.

Suriano, R., Zandrini, T., De Marco, C., Osellame, R., Turri, S., Bragheri, F., 2016. Nanomechanical probing of soft matter through hydrophobic AFM tips fabricated by two-photon polymerization. Nanotechnology 27 (15). https://doi.org/10.1088/0957-4484/27/15/155702.

Swain, M.V., Nohava, J., Eberwein, P., 2017. A simple basis for determination of the modulus and hydraulic conductivity of human ocular surface using nano-indentation. Acta Biomater. 50, 312–321. https://doi.org/10.1016/j.actbio.2016.12.007.

Tibbitt, M.W., Anseth, K.S., 2009. Hydrogels as extracellular matrix mimics for 3D cell culture. Biotechnol. Bioeng. 103 (4), 655–663. https://doi.org/10.1002/bit.22361.

Tsui, T.Y., Pharr, G.M., 1999. Substrate effects on nanoindentation mechanical property measurement of soft films on hard substrates. J. Mater. Res. 14 (1), 292–301. https://doi.org/10.1557/JMR.1999.0042.

V Derjaguin, B., Muller, V.M., Toporov, Y.P., 1975. Effect of contact deformations on the adhesion of particles. J. Colloid Interface Sci. 53 (2), 314–326.

Wang, Z., Volinsky, A.A., Gallant, N.D., 2015. Nanoindentation study of polydimethylsiloxane elastic modulus using berkovich and flat punch tips. J. Appl. Polym. Sci. 132 (5), 1–7. https://doi.org/10.1002/app.41384.

Wyss, C.S., Karami, P., Bourban, P.E., Pioletti, D.P., 2020. Hybrid granular hydrogels: combining composites and microgels for extended ranges of material properties. Soft Matter 16 (15), 3769–3778. https://doi.org/10.1039/d0sm00213e.

Xue, H., et al., 2019. Quaternized chitosan-Matrigel-polyacrylamide hydrogels as wound dressing for wound repair and regeneration. Carbohydr. Polym. 226 (September), 115302 https://doi.org/10.1016/j.carbpol.2019.115302.

Zant, E., Blokzijl, M.M., Grijpma, D.W., 2015. A combinatorial photocrosslinking method for the preparation of porous structures with widely differing properties. Macromol. Rapid Commun. 36 (21), 1902–1909. https://doi.org/10.1002/marc.201500229.

Zhi Li, D.B., Gao, Sai, Brand, Uwe, Hiller, Karla, Hahn, Susann, Hamdana, Gerry, Peiner, Erwin, Wolff, Helmut, 2019. Nanomechanical characterization of vertical nanopillars using an MEMS-SPM nano-bending testing platform. Sensors 19 (20), 4529.

Zhu, Y., Dong, Z., Wejinya, U.C., Jin, S., Ye, K., 2011. Determination of mechanical properties of soft tissue scaffolds by atomic force microscopy nanoindentation. J. Biomech. 44 (13), 2356–2361. https://doi.org/10.1016/j.jbiomech.2011.07.010.